Destroy, create, transform and sublimate: laboratory dissociation studies on polycyclic aromatic hydrocarbons and analogues

Kamer, J.

2 Methodology

The data presented in this thesis is measured using a variety of systems. This chapter will present those systems and give a description of their general workings and important components, in addition to the concise descriptions in the related chapters.

2.1 i^2PEPICO system

The experiments presented in **Chapter 3** were conducted on a double imaging photoelectron photoion coincidence (i^2PEPICO) spectrometry instrument situated at the vacuum ultraviolet (VUV) beamline of the Swiss Light Source (SLS), which is part of the Paul Scherrer Institute (PSI). This system, see Fig. 2.1 for a schematic overview, allows for mass spectrometric and photoelectron spectroscopic measurements to study reactivity and reveal reaction dynamics, as well as isomer identification. A detailed description of the system is given in Johnson *et al.* (2009); Bodi *et al.* (2012); Sztáray *et al.* (2017). In this experiment, neutral molecule are photoionized by monochromatic radiation coming from the SLS synchrotron. Electrostatic lenses transport both the resulting electrons and ions in opposite directions. Upon detection, the position of the electrons is mapped onto a MCP RoentDek delay-line imaging detector, and their arrival time provides the start signal for the time-of-flight (TOF) analysis of the coincident photoions. These were space focused onto a second MCP RoentDek delay-line imaging detector, and their delayed coincidence arrival time provides information on their mass-to-charge ratio (m/z). Electrons with zero kinetic energy (ZKE), i.e. electrons that contain no excess energy after ionization, also called threshold electrons, generally arrive at the center of the MCP. Due to position mapping, these electrons

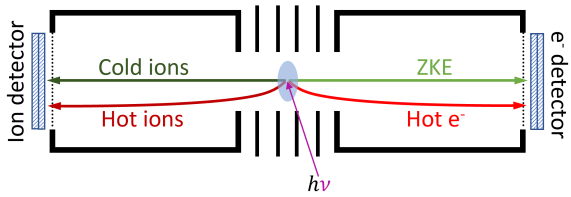

Figure 2.1: Schematic of an i^2PEPICO spectroscopy system. Neutral molecules (blue oval) are irradiated with VUV light, originating from the synchrotron, which ionizes the molecules. The cation and electron are transported in opposite directions by static electronic lenses. When an electron hits the detector a timer is started that ends when the ion is detected, effectively giving a time-of-flight (TOF) spectrum. The charged particles are detected by Roentdek DLD40 detectors, which also allow for electron and cation selectivity, see text.

can be isolated from the data, thus probing only the molecules/ions that absorbed all of the photon energy. However, "hot" electrons, i.e. electrons with non-zero kinetic energy, are also occasionally imaged onto the center spot of the detector, while mainly these would arrive away from the center of the MCP. The "hot" electrons can be compensated for by selecting a ring, surrounding the center region circle, of electrons and subsequently subtracting the resulting coincidence mass spectrum multiplied with factor f from the mass spectrum resulting from the center electrons:

$$I_{\mathrm{Comp}} = I_{\mathrm{Circ}} - f \cdot I_{\mathrm{Ring}}. \tag{2.1}$$

The factor f is the ratio between the areas of the center circle and the ring, $f = \frac{r^2_{\mathrm{Circ}}}{r^2_{\mathrm{ring}} - r^2_{\mathrm{Circ}}}$, which is generally set to ~ 0.3 (Sztáray & Baer 2003; Bodi & Hemberger 2014).

The TOF mass spectrometer is fit with two acceleration regions. One is specifically put at a low draw out potential, which allows ions that dissociate on the μs timescale to do so in this region. When this occurs, the resulting fragment ion will arrive later on the MCP than it would when the dissociation had partaken before entering the TOF region, resulting in an asymmetric TOF mass peak towards longer times/higher masses. This data can be modeled by feeding miniPEPICO (Sztáray *et al.* 2010), custom made data fitting program software, the energy en vibrational data from calculated ions (see section 2.3). The resulting model gives the unimolecular decay rate constants as a function of photon energy of the molecules of interest, and can be used to analyze reactivity and dissociative photoionization processes.

2.2 Quadrupole ion traps

The other chapters in this thesis present experimental data measured on quadrupole ion trap (QIT) systems. The work done in **Chapter 4** utilizes the QIT user station of Free-Electron Lasers for Infrared eXperiments (FELIX). This system comprises of the commercially available Bruker Amazon Speed ETD, detailed description in Martens *et al.* (2016), which has been adjusted to facilitate IR light from FELIX to enter the QIT. Ions are generated in an electronspray ionization (ESI) source. An intricate set of electronic optics and pressure differences transports the ions into the ion trap, where they can be irradiated with IR light from FELIX. With IR light, the so-called infrared multiple photon dissociation (IRMPD) technique can be used to study the IR spectra of the ions. Voltage ramping extracts the ions from the trap, allowing for their detection.

In the last two chapters the experimental work is performed on the Instrument for the Photoprocessing of PAHs (i-PoP), an in-house QIT in the Laboratory for Astrophysics (LfA) in Leiden. i-PoP is a custom-made QIT system mainly built from Jordan TOF Products, Inc. components (Zhen *et al.* 2014a). A schematic of the system is presented in Fig. 2.2/ The system comprises out of two vacuum chambers: the source chamber where the ions are generated, trapped and irradiated, and the detection chamber, which houses a reflectron time-of-flight (re-TOF) mass spectrometer (Jordan D-850). In the source chamber, a PA(N)H sample is put in the oven (Heat Wave Labs) and is gently sublimated by increasing the oven temperature. When in the gas-phase, the PA(N)Hs are ionized via electron impact from an electron gun (E-gun; Jordan C-950) and subsequently guided into the QIT (Jordan C-1251). Filling of the QIT is

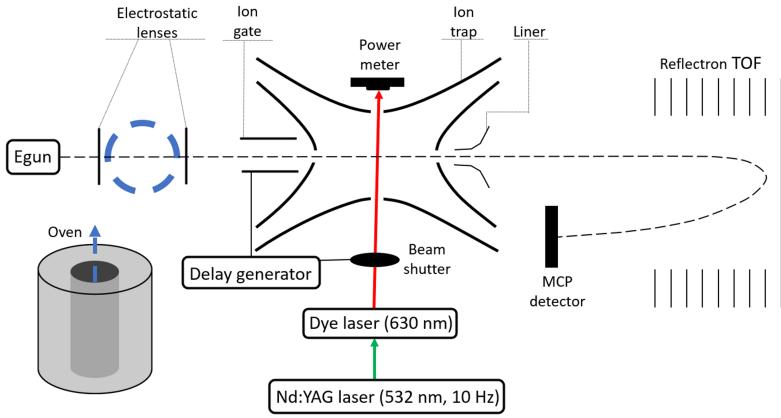

Figure 2.2: Schematic of the i-PoP system at the Laboratory for Astrophysics at Leiden University. This schematic represents the general workings of an QIT system. A sample is sublimated and subsequently ionized with an electron gun. The cations are transported into the QIT by electrostatic lenses. After irradiation in the QIT, the cations and fragments are extracted and detected using the reflectron time-of-flight technique on a z-gap multichannel plate detector. Figure made by Iris Elfferich.

controlled with an ion gate, by switching an electronic lens to a high negative/positive voltage. In the QIT ions can be irradiated by a dye laser (LIOP-TEC, Quasar2-VN) that was pumped by a 10 Hz Nd:YAG (Quanta-Ray, INDI-40-10). The dye laser was filled with the dye 4-(dicyanomethylene)-2-methyl-6-(4-dimethylaminostyryl)-4H-pyran (DCM) dissolved in ethanol and tuned to a wavelength of 630 nm, which is around the most energetically intense wavelength of DCM. The dissociation products are extracted by applying a positive and negative voltage on the repeller and extractor endcaps, respectively. After traversing the re-TOF, the ions are detected on a z-gap multichannel plate (MCP) detector.

In this section a more detailed description of the inner workings of a QIT system will be given that encompasses both used QIT systems.

2.2.1 Ion trapping

A QIT is made up of a central electrode ring with two hyperbolic metal electrodes at each end. If an AC, radiofrequency (RF), voltage is applied to the ring electrode, ions can be trapped in the QIT. The ions that can be effectively trapped are limited by their stability inside the trap, characterized by the stability parameter β_u, where u depicts either radial stability parallel to the ring electrode (r) or stability perpendicular to the ring electrode (z). Ions typically fall out of the stability region more quickly in the z-direction than in the radial direction. Consequently, in most quadrupole ion trap (QIT) experiments, only the z-direction is considered of importance. Hence, only the stability in the z-direction will be further elaborated. When $\beta_z \leq 1$ ions will be stable in the QIT. For a *grounded* QIT – which is the case for both QITs used in this thesis

– β_z is defined precisely as a continued fraction expression: (March 1997)

$$\beta_z^2 = \frac{{q_z}^2}{(\beta_z+2)^2 - \frac{{q_z}^2}{(\beta_z+4)^2 - \frac{{q_z}^2}{(\beta_z+6)^2-\ldots}}} + \frac{{q_z}^2}{(\beta_z-2)^2 - \frac{{q_z}^2}{(\beta_z-4)^2 - \frac{{q_z}^2}{(\beta_z-6)^2-\ldots}}}, \tag{2.2}$$

where q_z is a Mathieu equation parameter, which follows from the properties of the QIT: (March 1997)

$$q_z = \frac{4eV_{\mathrm{RF}}}{m\,({r_0}^2 + 2{z_0}^2)\,\Omega^2}, \tag{2.3}$$

where e is the elementary charge, V_{RF} is the peak-peak amplitude of the RF voltage applied to the ring electrode, m is the mass of the ion of interest, r_0 is the ring electrode radius, z_0 is half the distance between the two end cap electrodes and Ω represents the angular frequency of the RF voltage (in rad s^{-1}). In order for the $\beta_z \leq 1$ condition to be met, q_z must be ≤ 0.908.

While stable in the ion trap, ions will follow a trajectory similar to a Lissajous curve composed of two frequency components ω_r and ω_z, which are given by (March 1997)

$$\omega_{u,n} = \begin{cases} (n + \frac{1}{2}\beta_u)\Omega & 0 \leq n < \infty \\ -(n + \frac{1}{2}\beta_u)\Omega & -\infty < n < 0. \end{cases} \tag{2.4}$$

Normally, only the fundamental frequency ($n = 0$) is of importance, for instance for mass isolation (see section 2.2.2), therefore eq. (2.4) can be reduced to:

$$\omega_{u,0} = \frac{1}{2}\beta_u\Omega. \tag{2.5}$$

In most QIT systems, excess kinetic energy of the trapped ions is reduced by leaking a buffer gas, mainly helium, into the QIT. The energetically excited ions will collide with the buffer gas, which thermalizes them to about room temperature. This reduces the size of the ion cloud, thus increasing the ion density, resulting in an increased trapping efficiency and a better mass resolution when the ion cloud is measured. However, the introduction of a buffer gas effects the frequency of the trapped ion trajectories (Guan & Marshall 1993). This frequency should now be affected by a (arbitrary) collisional damping coefficient γ_u, that describes the interaction between the ions and the buffer gas. The "new" frequency $\omega'_{u,0}$ is given by (Guan & Marshall 1993)

$$\omega'_{u,0} = \frac{\sqrt{4(\omega_{u,0})^2 - {\gamma_u}^2}}{2}. \tag{2.6}$$

2.2.2 Mass isolation

An unfortunate side effect of using electron impact for ionization is the partial fragmentation of the sample ions. Although this is mostly limited to loss of a few hydrogen atoms, some PA(N)Hs can lose bigger fragments as well (see black trace in Fig. 2.3). Furthermore, contaminations from previous experiments and from sample synthesis, may also be present in the trap. The resulting peaks, when not accounted for, can trouble the analysis as it becomes unclear if an ion is created, for instance, from electron impact fragmentation or laser irradiation, or if it is a contaminant. To absolve this issue, ions in a QIT can be isolated by the use of a stored waveform inverse Fourier

transform (SWIFT) pulse (Doroshenko & Cotter 1996). This pulse is a time-discrete waveform that is created from the inverse Fourier transform of an excitation spectrum that coincides with the frequencies ($\omega'_{u,0}$) of the undesirable ions. The (time-discrete) SWIFT pulse at $t_i = i\delta t$, where δt is the sampling interval and $i = 0, 1, \ldots, (N-1)$, is described by (Doroshenko & Cotter 1996)

$$U_i = \sum_{k=k_{\min}}^{k_{\max}} A_k \cos\left(-\frac{2\pi ik}{N} + \varphi_k\right), \tag{2.7}$$

where A_k is the amplitude of the k-th frequency component with a frequency (in Hz) $f_k = k\delta f$, with δf defined as $\delta f = \frac{1}{N\delta t}$ and φ_k is the phase of the k-th frequency component. Generally, A_k is either 0 or 1, depending on if an ion needs to be retained in the ion trap or expelled, respectively. $k_{\min,\,\max}$ are defined using the frequency interval $f_{\min}$ to $f_{\max}$ as $k_{\min,\,\max} = \frac{f_{\min,\,\max}}{\delta f}$. When $\omega'_{u,0}$ lies outside of this frequency range, the ion is not affected by SWIFT, and will thus be retained. The phase for each k-th component is described by (Doroshenko & Cotter 1996)

$$\varphi_k = \frac{1}{2}\pi\left(k + \frac{k^2}{k_{\max} - k_{\min} + 1}\right). \tag{2.8}$$

The SWIFT pulse is applied to one of the end cap electrodes of the QIT. Ions of which their $\omega'_{u,0}$ coincides with the excitation spectrum will be expelled from the ion trap. This effect can clearly be seen in Fig. 2.3, where a SWIFT pulse was constructed such that $A_k = 0$ for the ions in the m/z $301 - 305$ and $A_k = 1$ for the remaining frequencies within the interval. Moreover, expelling ions from the ion trap reduces the amount of space charge, hence allowing for a denser ion cloud and an improved mass resolution. Also, combining SWIFT with a varying V_{RF} can be used as a valuable analytical technique, as is shown in **CHAPTER 6**.

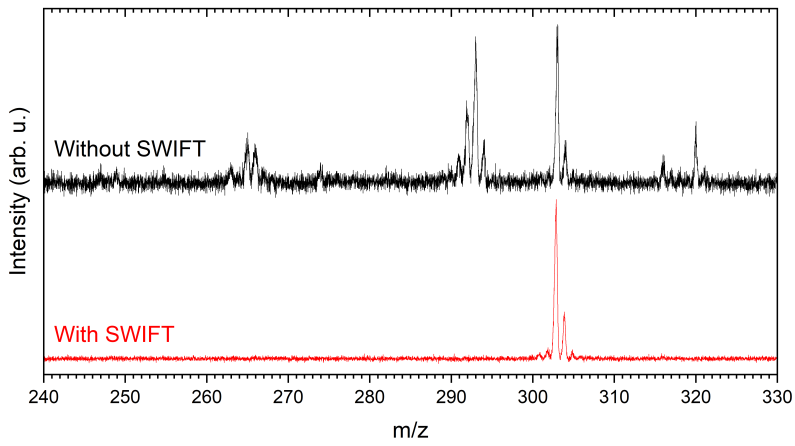

Figure 2.3: An example of the effectiveness of the SWIFT mass isolation technique. The black spectrum is a measurement of a $\mathbf{TAC}^{\bullet+}$ sample (m/z 303, see **CHAPTER 5**) without any applied SWIFT pulse and the red spectrum shows the $\mathbf{TAC}^{\bullet+}$ measurement with an applied SWIFT pulse. The dissociation in both spectra is induced by the E-gun. Both spectra are normalized with respect to the $\mathbf{TAC}^{\bullet+}$ parent peak intensity.

2.2.3 Infrared multiple photon dissociation

The IRMPD technique (summarized in Fig. 2.4) is generally used to acquire an experimental IR spectrum of an ion and to identify a certain isomer (Polfer & Oomens 2007). Both of these applications of IRMPD are utilized in **Chapter 4**. The IRMPD technique relies on the energy redistribution of the studied ion. PA(N)Hs are known to redistribute the energy, through internal conversion and intramolecular vibrational distribution, into its vibrational modes when a photon is absorbed. In the ISM a PA(N)H subsequently releases this energy by emitting IR photons (Allamandola *et al.* 1989). However, this process can be exploited in reverse. A resonant IR photon can be absorbed by the ion, putting it in an excited state. This energy is then redistributed over the ion's bath of vibrational modes, making it possible for the absorption of another resonant IR photon. This process continues until some vibrational modes are sufficiently filled and the only way to release this energy is to dissociate. When an IR photon is off-resonance with the ion, it is less likely to be absorbed and, therefore, little to no dissociation will happen. This allows the dissociation to be indicative of the vibrational modes of an ion. The IRMPD yield is defined as the ratio between the intensity of all fragments and the total intensity of all fragments and the parent ion:

$$\text{Yield}_{\text{IRMPD}} = \frac{\sum I_f}{\sum I_f + I_p}. \tag{2.9}$$

Scanning over an IR wavelength region and calculating the IRMPD yield for each wavelength leads to an IRMPD spectrum of our ion of interest.

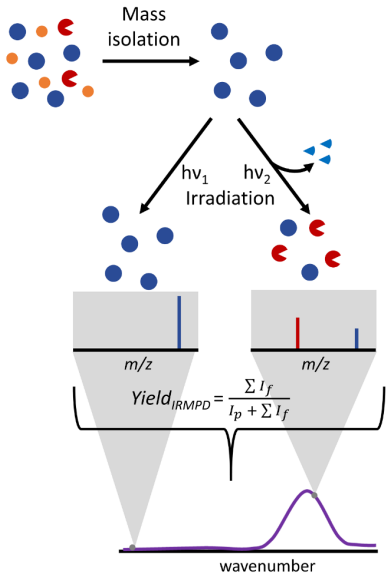

Figure 2.4: Illustration of the process of the IRMPD technique. First, ions are created and the ion of interest is mass isolated and are subsequently irradiated with IR light. When the IR light is not resonant with the ion's vibrational modes, no dissociation is observed. In resonance, the ion will dissociate. The IRMPD yield is the intensity of all dissociation fragments divided by the total intensity of all peaks (Carlo & Patrick 2022).

2.2.4 Mass spectrometry

After mass isolation and photoprocessing, the ion remaining in the trap must be extracted for detection. There are several ways to extract and detect ions in order to create a mass spectrum, however in this work only the extraction and detection methods of the used instruments will be described.

2.2.4.1 Voltage ramping

To create a mass spectrum, the FELIX QIT system extracts its ions by ramping V_{RF}. In order for an ion to be removed from the trap its stability parameter q_z must be higher than 0.908. Putting this value into eq. (2.3) and rewriting it such that $\frac{m}{e}$ is isolated, a linear dependence of the extracted ion mass m with V_{RF} becomes apparent:

$$\frac{m}{e} = V_{\mathrm{RF}} \cdot \frac{4}{\left(r_0{}^2 + 2z_0{}^2\right)\Omega^2 \cdot 0.908} \Rightarrow \frac{m}{e} = V_{\mathrm{RF}} \cdot C. \tag{2.10}$$

The extracted ions are detected as a current as function of time, $I\left(t\right)$ using a conversion dynode detector. Since the amplitude of V_{RF} is ramped over a certain time, $V_{\mathrm{RF}}\left(t\right)$, the measured current can be linked to $V_{\mathrm{RF}}\left(t\right)$, effectively giving the measured current as function of V_{RF}. This is subsequently mass calibrated using eq. (2.10), resulting in a mass spectrum.

2.2.4.2 Reflectron Time-of-flight

The i-PoP system extracts the ions from the QIT by slowly lowering V_{RF} to 0 V and subsequently putting a high voltage on both endcaps simultaneously. Generally, a voltage of about +800 and −800 V is put on the repeller and extractor endcap, respectively, effectively exposing them to an electric field, Φ. This guides the ions out of the QIT into a field-free TOF region. Since it is a field-free region, all of the electric potential energy is converted to kinetic energy:

$$e\Phi(\mathbf{r}) = \frac{1}{2}mv^2, \tag{2.11}$$

where $\mathbf{r}$ is the position of an ion in the QIT. v can be converted into the flight length, d, divided by the flight time, t, of the ion of interest. This can be rewritten to give the mass-to-charge ratio as function of the flight time:

$$\frac{m}{e} = t^2 \cdot \frac{2\Phi(\mathbf{r})}{d^2}. \tag{2.12}$$

With this equation the measured intensity as a function of time can be calibrated to be as a function of mass-to-charge ratio. Typically, the mass-to-charge ratio is depicted using a z instead of e, as an ion could potentially be multiply charged.

Inside the QIT, ions can have different velocity distributions, meaning that when they are extracted they already contain some kinetic energy. This leads to a bad mass resolution ($\frac{m}{\Delta m}$), as more energetic particles arrive earlier on the detector and less energetic particles later. This can be compensated for by building a reflectron stage in the TOF (re-TOF), where more energetic ions penetrate deeper into the reflectron potential, therefore traversing a longer flight path, which allows the less energetic ones to catch up and arrive on the detector at the same time. As this is not a linear TOF

system, eq. (2.12) cannot be used for mass calibration. The mass calibration equation for a re-TOF is not easily derived but comes down to the following relation: (Gasc *et al.* 2017)

$$\frac{m}{z} = \left(\frac{t - t_0}{C}\right)^2, \tag{2.13}$$

where t_0 and C are constant parameters that can be calculated using

$$t_0 = \frac{\sum_{i=1}^{N}\left(\sqrt{m_i}t_i\right)\sum_{i=1}^{N} t_i - \sum_{i=1}^{N}\sqrt{m_i}\sum_{i=1}^{N} {t_i}^2}{N\sum_{i=1}^{N}\left(\sqrt{m_i}t_i\right) - \sum_{i=1}^{N}\sqrt{m_i}\sum_{i=1}^{N} t_i}, \tag{2.14}$$

and

$$C = \frac{N\sum_{i=1}^{N} {t_i}^2 - \left(\sum_{i=1}^{N} t_i\right)^2}{N\sum_{i=1}^{N}\left(\sqrt{m_i}t_i\right) - \sum_{i=1}^{N}\sqrt{m_i}\sum_{i=1}^{N} t_i}, \tag{2.15}$$

in which N is the number of reference ion peaks ($N \geq 2$), t_i is the time of flight of the i-th peak and m_i is the associated mass. This allows for the mass calibration using multiple peaks, which enhances the accuracy of the calibration. When only two ion peaks are used for calibration, for instance the parent ion and a hydrogen loss peak, t_0 and C can be reduced to:

$$t_0 = \frac{\sqrt{m_1}\cdot t_2 + \sqrt{m_2}\cdot t_1}{\sqrt{m_1} - \sqrt{m_2}} \quad \text{when } N = 2, \tag{2.16}$$

and

$$C = \frac{t_1 - t_2}{\sqrt{m_1} - \sqrt{m_2}} \quad \text{when } N = 2. \tag{2.17}$$

The recorded mass spectra can be analyzed by integrating the peak area. The resulting intensities allow for the quantitative analysis of the data by constructing a breakdown diagram. Individual peaks are first fitted with a model function instead of numerical integration, as the former compensates for small statistical variations in the data and noise. Generally, Gaussian functions are used to fit mass peaks and they provide a relatively good fit, see Fig. 2.5, although, a Gaussian distribution does not take into account the asymmetry and skewness of the data. A more proper fit is obtained by using a Pearson type IV probability distribution: (Pearson 1895)

$$p(x) = \frac{\left|\frac{\Gamma\left(m+\frac{\nu}{2}i\right)}{\Gamma(m)}\right|^2}{\alpha \mathrm{B}\left(m-\frac{1}{2},\frac{1}{2}\right)}\left[1+\left(\frac{x-\lambda}{\alpha}\right)^2\right]^{-m}\exp\left[-\nu\arctan\left(\frac{x-\lambda}{\alpha}\right)\right], \tag{2.18}$$

where the first component is a parameter related to the peak intensity, α is the scale parameter, m is the shape parameter, λ is the location parameter and ν controls the skewness. Γ and B are the Gamma and Beta functions, which are defined as:

$$\Gamma(z) = \int_0^\infty x^{z-1}e^{-x}dx, \tag{2.19}$$

and

$$\mathrm{B}(x,y) = \frac{\Gamma(x)\Gamma(y)}{\Gamma(x+y)}. \tag{2.20}$$

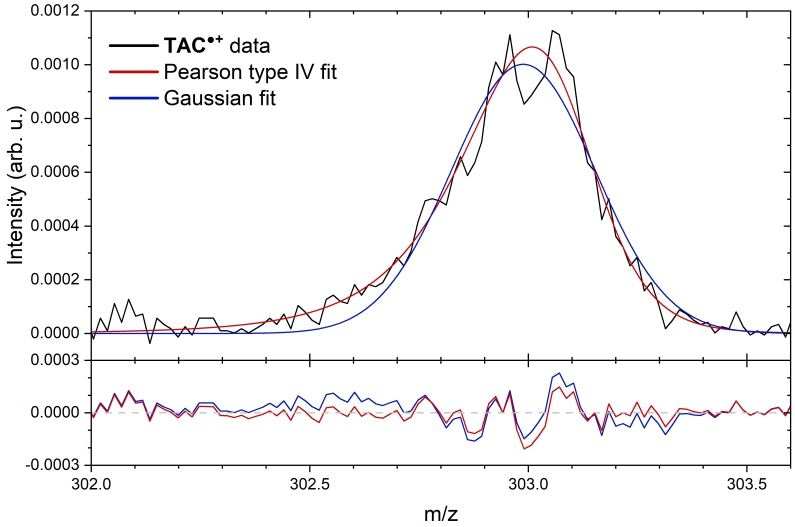

Figure 2.5: Comparison of a Pearson IV type fit (red) to a Gaussian fit (blue) to the parent peak of a $\mathbf{TAC}^{\bullet+}$ measurement. The fits and residuals are shown in the top and bottom panel, respectively. Both fit the peak relatively well, however the peak shoulders are better accounted for with the Pearson type IV fit. Originally, the fit is performed on the TOF data and later calibrated to m/z.

Since the data obtained from the MCP is in voltage we need a conversion factor, χ, from the unitless probability distribution $p(x)$:

$$V_{\text{fit}}(t) = p(t) \cdot \chi. \tag{2.21}$$

Here, $\chi \in \mathbb{R}$ which is determined for each peak individually. Since the first component of eq. (2.18) is also $\in \mathbb{R}$ and, moreover, quite challenging to calculate, it can be combined with χ to make a new conversion factor χ':

$$\chi' = \chi \cdot \frac{\left|\frac{\Gamma\left(m+\frac{\nu}{2}i\right)}{\Gamma(m)}\right|^2}{\alpha \mathrm{B}\left(m-\frac{1}{2},\frac{1}{2}\right)}. \tag{2.22}$$

Now, the Γ and B functions do not have to be calculated and the final fitting equation is as follows:

$$V_{\text{fit}}(t) = \chi' \left[1+\left(\frac{t-\lambda}{\alpha}\right)^2\right]^{-m} \exp\left[-\nu \arctan\left(\frac{t-\lambda}{\alpha}\right)\right]. \tag{2.23}$$

A custom made Matlab program automatically adjusts the χ', α, m, λ and ν parameters such that eq. (2.23) fits the data most optimally. All fits in this work are performed on the uncalibrated TOF data, i.e. intensity versus time. Fig. 2.5 shows a comparison between a Gaussian distribution fit and a Pearson type IV distribution fit. On first sight both fit the data relatively well, however when considering the shoulders of the asymmetric peak, the Pearson type IV fit is significantly better.

2.3 Computational

Experimental works are crucial to our understanding of the ISM and its chemistry. However, they do have their limitations, mainly regarding time constraints and technical limitations, for instance temperature and pressure. Furthermore, radical neutral molecules, which are likely present in the ISM, are impossible to synthesize under the atmospheric conditions present on earth. Quantum chemical calculation are an excellent way to circumvent these issues and can be used as a control and/or comparison to the experimental data to improve experimental scientific conclusions. Of the many theoretical tools that are to our availability, density functional theory (DFT) is primarily used in this work.

The Schrödinger equation is at the base of all quantum chemical calculations, as it harbors all information on a molecule's electronic, vibrational and rotational energy levels. However, only the most simple systems have an analytical or numerical solution, thus quantum chemical calculations of bigger systems require approximations. One crucial approximation is the Born-Oppenheimer approximation, which states that the wave functions of atomic nuclei and the electrons in a molecule can be dealt with independently, due to the fact that the nuclei are significantly heavier than the electrons. Therefore, the coordinates of the nuclei in a system can be approximated as fixed, while the electron coordinates are dynamic. Now, it is possible to solve the Schrödinger equation separately for the nuclei and the electrons.

To further aid the calculation, DFT replaces the individual electron wave functions by an electron density, that is described by a linear combination of functions that are comprised in a so-called basis set. Also, the electronic energy, and nuclei-electron and electron-electron interactions are replaced by functionals of the electron density. This part of the Schrödinger equation can now be calculated with relative ease. When solved, the nuclei coordinates can subsequently be (slightly) readjusted, and a new calculation of the electron Schrödinger equation is performed. This is done iteratively until convergence of the system. Several basis sets and functionals, each with their own properties, are available for these calculations and should be chosen carefully to best represent the system's characteristics, while also maintaining an acceptable computation time and accuracy (Karton 2017; Witte *et al.* 2016).

The main two results coming from these types of calculations are the energy of the ion/molecule and its vibrational modes. The former can be used to calculate bond dissociation energies (BDEs), for instance from the hydrogen atom loss of a PA(N)H. If the energy of the lone hydrogen atom and the resulting molecular structure after hydrogen loss are both subtracted from the initial molecule, the BDE is acquired. Furthermore, the energy required for isomerizations can also be determined, and also the transition states that are involved in isomerizations and dissociations. All of this combined can be used to create a potential energy surface (PES), that describes the entire reaction from reactants to products both geometrically as energetically. The calculated vibrational modes are a hint towards the expected IR photon radiation/absorption of a molecule or ion. As an example, these modes can be used for isomer identification if an experimental IR spectrum if available for a reaction with unknown products. Normally, the vibrational modes of molecules and ions are described by an anharmonic potential well, which takes considerably more time to calculate compared to a harmonic potential well. Therefore, DFT generally considers a harmonic approximation of the vibrational modes, thus meaning the calculated modes are slightly off. How-

ever, this can be compensated for by scaling the frequencies, depending on the modes and functionals and basis sets used, which appears to be sufficiently accurate to make proper conclusions (Andersson & Uvdal 2005). In this work, all DFT calculations are performed using the harmonic approximation and are scaled using proper scaling factors.